Searches for long-lived particles in ATLAS

Sascha Mehlhase[*]

on behalf of the ATLAS Collaboration
Ludwig-Maximilians-Universität München
E-mail: sascha.mehlhase@physik.uni-muenchen.de

Particles beyond the Standard Model can generally have life times that are long compared to Standard Model particles at the weak scale. When produced at the Large Hadron Collider, such long-lived particles can decay far from the primary interaction vertex and possibly themselves interact with the detector material, leading to a wide variety of detector signatures. Such long-lived particle signatures are distinctly different from those associated with searches for promptly decaying beyond-the-Standard Model particles that constitute the bulk of searches for new physics at the Large Hadron Collider, often requiring dedicated analysis and reconstruction techniques. This contribution will provide an overview for searches for long-lived particles performed by the ATLAS Collaboration and present latest results using 13 TeV proton–proton collision data from Run 2 of the Large Hadron Collider.

[*]Speaker.

1. Introduction

Hypothetical new particles predicted by theories beyond the Standard Model (SM) can generically have lifetimes that are long compared to SM particles at the weak scale. When produced at the Large Hadron Collider (LHC), such long-lived particles (LLPs) can decay far from the primary interaction vertex and possibly themselves interact with the detector material, leading to a plethora of possible detector signatures. Such LLP signatures are distinctly different from those associated with searches for promptly decaying beyond-the-SM (BSM) particles that constitute the bulk of searches for new physics at the LHC, often requiring dedicated analysis and reconstruction techniques. The latter can include the reconstruction of notably displaced decay vertices, *trackless jets*, tracks with anomalous properties, as well as short track segments.

The reasons for longevity of BSM particles are thereby essentially identical to those that create an enormous span in lifetime within the SM – from $\tau \sim 2 \cdot 10^{-25}$ s for the Z boson to the electron being stable – and include e.g. (nearly) mass-degenerate spectra or suppressed phase space available for decays in general, small couplings between the LLP and lighter states, highly virtual intermediate states, as well as (almost) conserved quantum numbers.

The fact that none of the searches for new physics at the LHC – predominantly looking for prompt signatures – have yet shown any clear signs of new particles, might also suggest to increase the effort in exploring non-promt and unconventional scenarios. Hereby it can be beneficial to address a given model – especially with intermediate lifetimes – with multiple analysis strategies, given the observed lifetime is governed by an exponential defined by the proper lifetime $c\tau$, leading to varying fractions of events decaying in different parts of the detector and thereby leaving diverse signatures.

Over the past years, the ATLAS Collaboration has increased its effort to cover a multitude of signatures of LLPs – from searches for heavy, stable, charged particles to closing the lifetime gap towards prompt searches. This contribution will focus on three recent examples covering a variety of different reconstruction and object-definition approaches as well as theoretical motivation, but also feature a general overview of the current status of searches for long-lived particle using 13 TeV LHC Run-2 proton–proton data collected with the ATLAS detector [1].

2. A search for heavy neutral leptons

Using up to 36.1 fb^{-1} of data, the ATLAS Collaboration performed a search [2] for heavy neutral leptons (HNLs) that are produced through mixing with muon or electron neutrinos and decay leptonically in a scenario with either lepton-number conservation (LNC) or lepton-number violation (LNV), as illustrated in Figure 1. These hypothetical right-handed neutrinos with Majorana masses below the electroweak scale could successfully address the problems of neutrino masses, matter–antimatter asymmetry and dark matter [3–6]. The results of this search are interpreted in a model postulating a single right-handed Majorana neutrino N produced in leptonic W-boson decays, with only two parameters: mass (m_N) and coupling strength ($|U|^2$). This search is a prime example of the complementarity of prompt and LLP approaches and utilises both signatures to set constraints on the HNL mixing to muon and electron neutrinos.
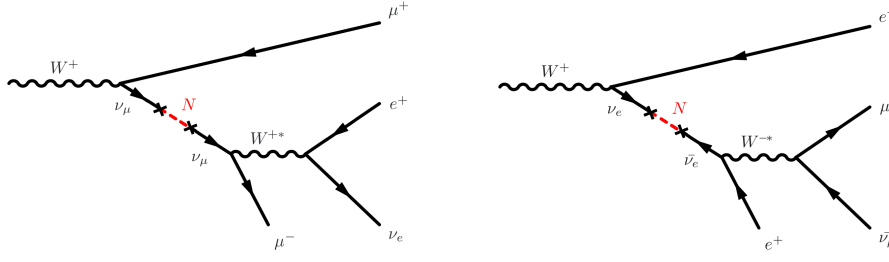
Figure 1: Examples of Feynman diagrams for HNL (N) production and decay in the channels this search is sensitive to: (left) μ mixing, $e\mu$ decay, LNC and (right) e mixing, $e\mu$ decay, LNV. [2]

The prompt signature, limited to LNV scenarios, requires three well reconstructed leptons produced at the interaction point (either $\mu^\pm\mu^\pm e^\mp$ or $e^\pm e^\pm \mu^\mp$) with – amongst other things – a veto on same-flavour opposite-charge topologies and requiring the three-lepton invariant mass ($m_{\ell\ell\ell'}$) between 40 and 90 GeV, while the displaced signature comprises a prompt muon from the W-boson decay and the requirement of a dilepton vertex (either $\mu\mu$ or $e\mu$) displaced in the transverse plane by 4–300 mm from the interaction point. Hereby the latter approach targets specifically low HNL masses ($m_N \lesssim 20$ GeV) where the searches relying on standard prompt objects become highly inefficient, as the HNL lifetime gets longer for lower masses and coupling strengths. Reconstructing a displaced vertex (DV) can not only compensate for this inefficiency, the requirement of a DV also eliminates most of the SM backgrounds, allowing to drop the requirement of same-charge same-flavour leptons and open the search to LNC scenarios.

The reconstruction of DVs at larger radial distances [7] with vertex masses $m_{\rm DV}$ down to 4 GeV is facilitated by a dedicated large-radius tracking (LRT) algorithm optimised for tracks with large unsigned transverse impact parameters relative to the primary interaction vertex (d0) [8], which – being computationally demanding – can only be run on a specifically preselected subset of the events rather than the entirety of the dataset.

The overall signal efficiency, depicted in Figure 2, depends on the mass and lifetime of the HNL and reaches about 10% at very short lifetime using the prompt signature to about 1–2% in the regions where the displaced signature takes over.

The background in the prompt search originates mostly from top–antitop, W+jets and multijet events where jets are accidentally misreconstructed as electrons or muons as well as from other contributions with two or more real leptons such as Z+jets, single-top-quark, diboson (WW, WZ and ZZ) and triboson events with hadronic decays. While W+jets, multijet and $t\bar{t}$ background are normalised using data in a simultaneous binned maximum-likelihood fit, with the $t\bar{t}$ shape extracted from MC simulation, the other background contributions are evaluated entirely from simulation. In the displaced search, possible background sources resulting in two-track DVs include hadronic interactions in material, decays of metastable particles such as b- and s-hadrons, accidental crossings of charged particles produced in the collisions, and cosmic-ray muons which either cross a charged particle from the collision or are reconstructed as two back-to-back displaced muons. Requiring the prompt muon in the same event reduces all of these backgrounds by more than an order of magnitude, requiring a tight lepton identification for all involved tracks further reduces all but the cosmic-ray muons background, which can be fully repressed by vetoing on back-to-back tracks. Other background from SM processes such as dijets and W+jets are estimated in a fully data-driven
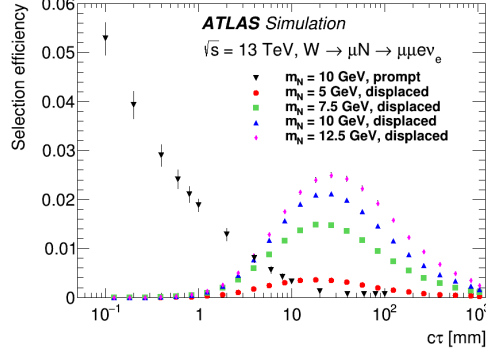
Figure 2: HNL search event selection efficiency as a function of mean proper decay length evaluated from simulation. The efficiency for the prompt signature in the muon channel is shown for an HNL mass of 10 GeV, while the efficiencies for the displaced signature are shown for four different HNL masses. Error bars represent MC statistical uncertainties. [2]
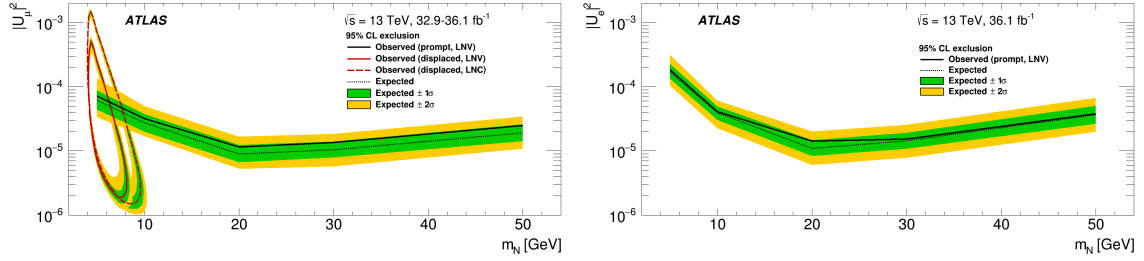

Figure 3: Observed 95% confidence-level exclusion in $|U_\mu|^2$ (left) and $|U_e|^2$ (right) versus the HNL mass for the prompt signature (the region above the black line is excluded) and the displaced signature (the region enclosed by the red line is excluded). The solid lines show limits assuming lepton-number violation (LNV) for 50% of the decays and the long-dashed line shows the limit in the case of lepton-number conservation (LNC). The dotted lines show expected limits and the bands indicate the ranges of expected limits obtained within 1σ and 2σ of the median limit, reflecting uncertainties in signal and background yields. [2]

manner using suitable control regions.

As no significant deviation from the background expectations is seen neither in the prompt nor in the displaced signatures, exclusion limits at the 95% confidence level are derived in a plane of HNL coupling strengths ($|U|^2$) and masses (m_N), as shown in Figure 3, in the cases of dominant mixing to ν_μ (left) and ν_e (right), for the cases of LNV (both signatures, solid lines) and LNC (displaced signature, long-dashed line).

The prompt signature sets limits in a mass range 5–50 GeV and excludes $|U_\mu|^2$ and $|U_e|^2$ above 1.4×10^{-5} in a mass range 20–30 GeV, while loosing sensitivity at higher masses due to a kinematic suppression of HNL production from the W-boson decay and at lower masses due to long decay path. Limits from the displaced signature cover the mass range 4.5–10 GeV and exclude coupling strengths down to $|U_\mu|^2 \sim 2 \times 10^{-6}$ (1.5×10^{-6}) assuming LNV (LNC), surpassing the best previous constraints using on-shell Z-boson decays from LEP1 [9] by one order of magnitude.

3

3. A search for neutral, long-lived scalars with signatures of displaced hadronic jets

Based on a dataset of up to 33.0 fb^{-1}, the ATLAS Collaboration sought [10] for pairs of neutral, long-lived scalars (s) with masses 5–400 GeV decaying mainly in the hadronic calorimeter (HCal) or at the outer edge of the electromagnetic calorimeter (ECal). In the considered simplified Hidden Sector (HS) [11–15] model, these scalars are thought to be produced from decays of heavy mediator bosons (Φ) with masses 125–1000 GeV and decay into SM fermions ($\Phi \to ss \to f\bar{f}f'\bar{f}'$), which – assuming the same branching ratios as those of the SM Higgs – are usually heavy fermions: $b\bar{b}$, $c\bar{c}$ and $\tau^+\tau^-$.

For intermediate lifetime, where the scalar decay occurs in the calorimeters, the two resulting quarks are reconstructed as a single jet, which – in contrast to SM processes – will usually have no associated activity in the tracking system, often a high ratio of energy deposited in the HCal to energy deposited in the ECal (*CalRatio* $= E_{\mathrm{HCal}}/E_{\mathrm{ECal}}$), and be reconstructed narrower than prompt jets when reconstructed with standard algorithms. This search requires two of these non-standard jets.

Already at the trigger level, this search takes advantage of two dedicated triggers making use of the three main characteristics of displaced jets: they are narrow jets, have a high fraction of their energy deposited in the HCal and typically have no tracks pointing towards the jet. At the hardware level, the search uses a high-E_{T} trigger targeting narrow energy deposits in both ECal and HCal and optimised for models with $m_\Phi > 200$ GeV as well as a low-E_{T} trigger targeting energy deposits with a large $E_{\mathrm{HCal}}/E_{\mathrm{ECal}}$ regaining efficiency for models with $m_\Phi \leq 200$ GeV. In the high-level trigger the same jet-cleaning algorithm, track-veto, and a cell-timing- and position-based algorithm to remove beam-induced background (BIB) [16] are applied to both initial setups. BIB hereby includes LHC beam-gas interactions as well as beam-halo interactions with the collimators upstream of the ATLAS detector, resulting in muons travelling parallel to the beam-pipe.

In the offline reconstruction, jets are classified as signal- or background-like jets using machine learning in two steps. First, for every reconstructed jet, the decay position of the particle that generated it is inferred using a multilayer perceptron, trained on signal jets from LLP decays, as shown in Figure 4 (left). Second, a per-jet Boosted Decision Tree (BDT) classifies jets as signal-like, multijet-like or BIB-like jets, as illustrated in Figure 4 (right). Subsequently events are then categorised as likely to have been produced by a signal process or a background process using a per-event BDT, trained separately for low and high m_Φ, with outputs shown in Figure 5.

Removing almost all the non-collision background, leaving only multijet background, and maximising the signal-to-background ratio in the final search region is achieved by making a selection on the relevant per-event BDT output value of candidate events and dedicated event quality criteria.

The main background contributions stem from SM multijet production, where jets are either mis-reconstructed due to noise or instrumental effects or composed mainly of neutral hadrons, or from non-collision background consisting of cosmic-ray muons and beam-induced background (BIB). The contribution from multijets is estimated using a data-driven ABCD method in a plane of jet–track separation $\sum \Delta R_{\mathrm{min}}(\mathrm{jet}, \mathrm{tracks})$ and the high/low-E_{T} per-event BDT output.

The data-driven background estimation and a signal hypothesis test are performed simultaneously in all regions and no excess of events is observed in the signal regions for either of the analysis
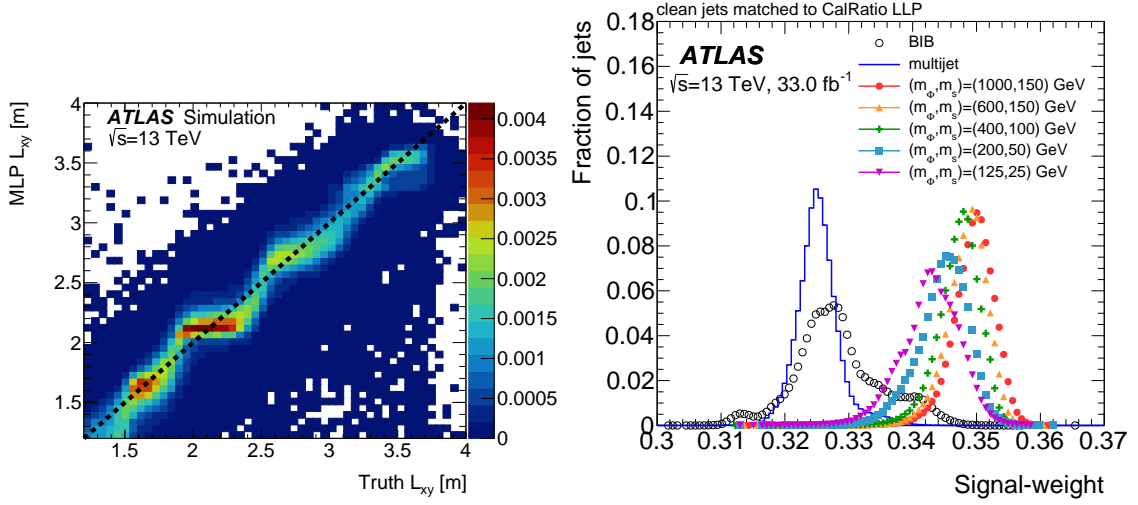
Figure 4: Left: Probability density of predicted MLP radial (L_{xy}) LLP decay positions as a function of the truth LLP decay positions, for reconstructed jets matched to the LLP. Dotted line shows where the MLP value equals the truth value. Right: The distributions of the per-jet BDT weights for a multijet sample, a BIB sample and five signal samples. For the signal samples, the weights for clean jets matched to an LLP decaying in the calorimeter are shown. The multijet and BIB distributions include weights for all clean jets in the event. [10]
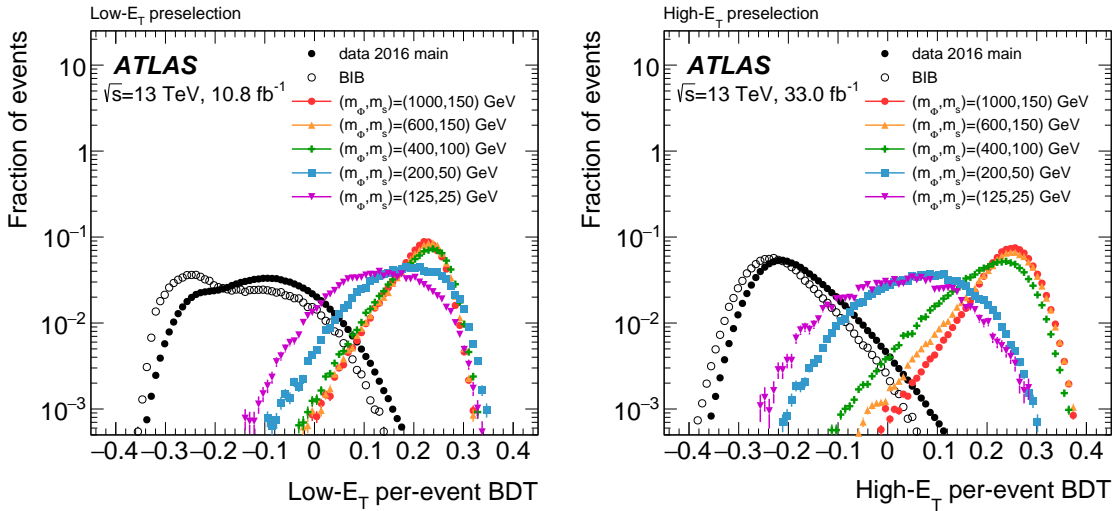
Figure 5: Distribution of the low-E_T per-event BDT (left) and high-E_T per-event BDT (right) on main data, BIB data and five signal samples after preselection. [10]
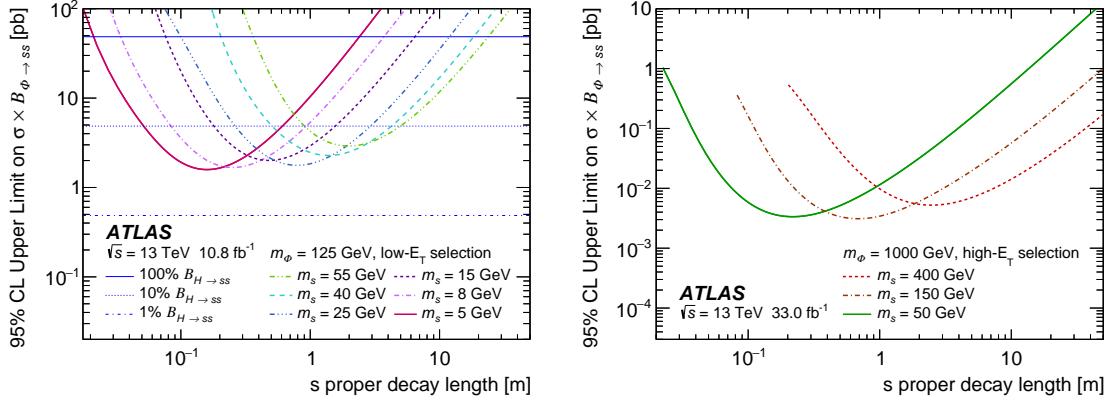
Figure 6: The observed limits for the Φ masses of 125 (left) and 1000 GeV (right). [10]
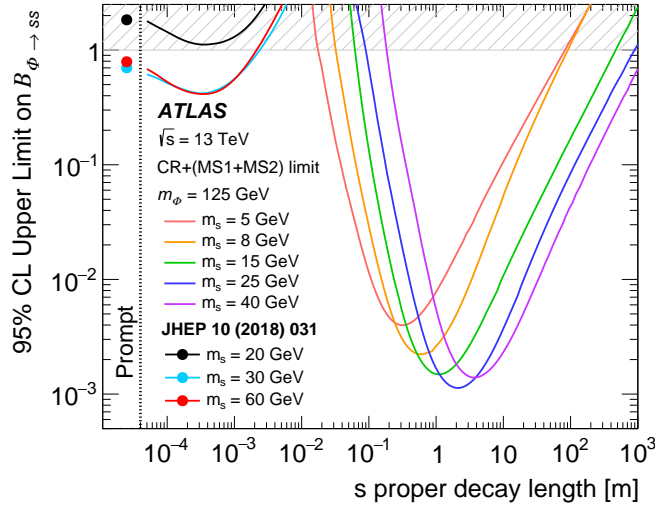

Figure 7: Summary of combined limits from the CalRatio (CR) analysis and the MS analysis for models with $m_\Phi = 125$ GeV, shown alongside limits from a $H \to aa \to 4b$ search. [10]

selections. Therefore exclusion limits at the 95% confidence level are set on $\sigma(\Phi) \times B_{\Phi \to ss}$ as a function of LLP decay length as shown in Figure 6 for different combinations of m_Φ and m_s. As an example, for a mediator like the Higgs boson, decays of neutral scalars with masses 5–55 GeV are excluded for proper decay lengths between 5 cm and 5 m depending on the LLP mass (assuming a 10% branching ratio).

A combination of the limits with the results of a similar ATLAS search [17] looking for displaced vertices in the muon spectrometer (MS), which is separated into the MS 1-vertex plus E_T^{miss} (MS1) and MS 2-vertex (MS2) components, yields limits that follow the most sensitive search for each mediator: the muon spectrometer limits for low-mass mediators with long decay lengths and the CalRatio limits for very short decay lengths. These are shown side-by-side with limits from a search for an exotic Higgs boson that decays into a pair of scalar particles which decay into b-quarks promptly or with a short lifetime [18] in Figure 7.
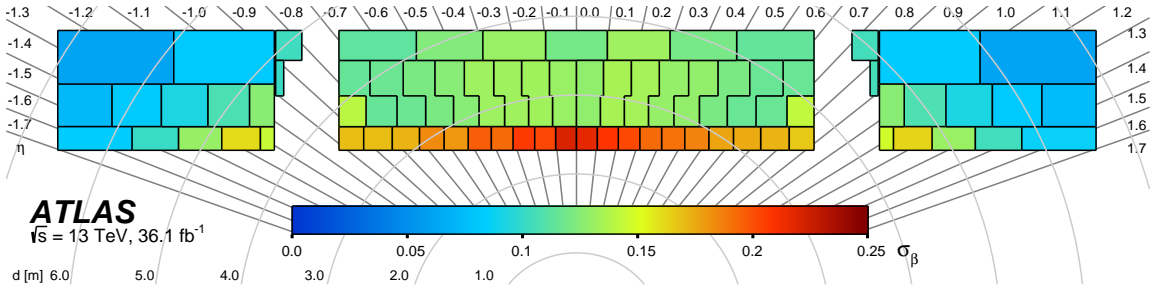
6

Figure 8: Resolution (σ_β) of the β measurement using muons for the different tile-calorimeter cells, which are shown with their actual shape. The grey circles indicate the distance from the interaction point and the grey straight lines the direction in η. [19]

4. A search for heavy charged long-lived particles

Using a dataset of 36.1 fb^{-1}, the ATLAS Collaboration conducted a search for heavy charged long-lived particles [19] that reach at least the hadronic calorimeter, based on observables related to ionisation energy loss (dE/dx) and time of flight (ToF), which are sensitive to the velocity of heavy charged particles travelling significantly slower than the speed of light. Predicted in a variety of theories that extend the SM, this search uses charged long-lived staus ($\tilde{\tau}$), squarks ($\tilde{q}$), gluinos ($\tilde{g}$) and charginos ($\tilde{\chi}_1^\pm$) as predicted by various supersymmetry models [20–30] as benchmark scenarios.

Both of the main observables used in this search require dedicated calibrations not performed centrally by the collaboration. For the dE/dx measurement performed in the innermost pixel detector, this includes η- and time-dependent corrections as well as a truncation procedure to reduce effects of the Landau tails on the estimate of the most probable value (MPV), which in turn is used in a three-parameter empirical function – calibrated using protons, kaons and pions with low transverse momentum – to obtain the $\beta\gamma$ of the particle. To obtain a β value from ToF measurements performed in the tile hadronic calorimeter as well as in the monitored drift tubes (MDTs) and resistive-plate chambers (RPCs) of the MS, the necessary calibrations – performed using muons in data – include corrections due to the Optimal Filtering Algorithm, geometry and η-dependence for each cell in the calorimeter and individual bias corrections for each of the drift tubes and readout strips in the MS. For all these systems a time-dependent correction corrects for long-term effects and the timing observed in simulation is adjusted to replicate the same resolution as observed in data. As an example, Figure 8 shows the resolution of the β measurement in the tile calorimeter after calibration and Figure 9 shows the fully-calibrated β resolution of β determined as a combination of the tile calorimeter, MDTs and RPCs.

Events are selected online through single-muon as well as missing-transverse-momentum triggers. While the former target mainly colour-neutral LLPs that reach the MS such as $\tilde{\tau}$ and $\tilde{\chi}_1^\pm$, the latter can – assuming the production of initial-state radiation gluons – compensate some of the efficiency loss due to late, out-of-time arrival of the particle in the MS and provide sensitivity for scenarios where the LLP does not reach the MS or turns neutral in the calorimeter. This *charge-flip* effect is only relevant for squarks and gluinos which hadronise into so-called *R*-hadrons and undergo hadronic interactions with the detector material, hence mainly in the calorimeters.
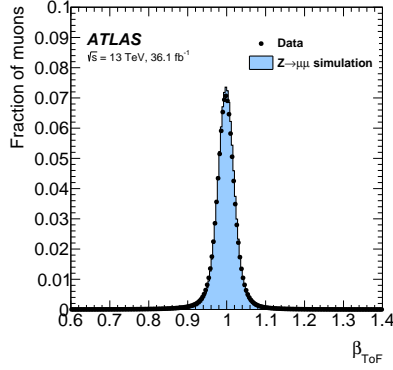
7

Figure 9: The β-distributions of muons for a $Z \to \mu\mu$ selection in data and simulation, with β measured as a combined measurement from RPCs, MDTs and tile calorimeter. [19]

The offline selection requires one or two candidates per event with an associated mass measurement derived from the β_{ToF} and – depending on the signal scenario – the $(\beta\gamma)_{dE/dx}$ measurement. Dedicated signal regions agnostic to all information from the MS, address *R*-hadron *charge-flip* scenarios and the fact that the exact nature of *R*-hadron hadronic interaction is still unknown.

The primary background contribution stems from high-momentum muons with mismeasured $\beta\gamma/\beta$ and is estimated in fully data-driven way by determining the probability density functions (pdfs) of the key variables momentum, β_{ToF} and $(\beta\gamma)_{dE/dx}$ – using sideband regions where possible – and randomly sampling the pdfs to obtain distributions of expected background in final selection variables m_{ToF} and – where applicable – $m_{dE/dx}$. Also the normalisation is derived from data using low-mass control regions. Examples of the background estimate for two different signal regions are shown in Figure 10.

No significant excess of observed data events above the expected background is found in the examined mass ranges and signal regions. Upper limits at 95% confidence level are placed on the production cross sections for various benchmark models, as shown in Figures 11 and 12. These results translate into lower limits on the masses of long-lived gluino, sbottom and stop *R*-hadrons, as well as staus and charginos of 2000 GeV, 1250 GeV, 1340 GeV, 430 GeV and 1090 GeV, respectively.
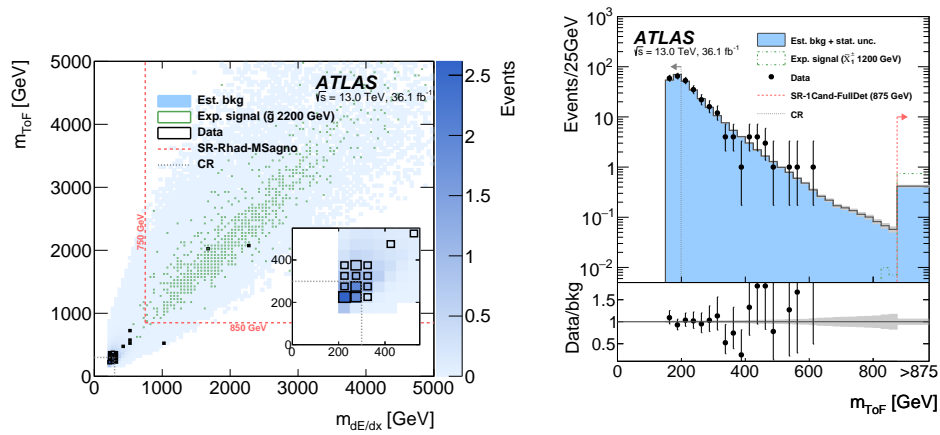
Figure 10: Background estimate for the MS-agnostic analysis targeting gluino *R*-hadrons in the $m_{\text{ToF}}-$ $m_{dE/dx}$ plane (left) and targeting pair-produced staus and charginos in a one-candidate SR (right). The dashed red lines indicate the lower bounds of the signal region for a representative signal choice, while the dotted grey lines illustrate the upper bound for the control region. The signal, a 2200 GeV gluino *R*-hadron (1200 GeV chargino) is indicated by green markers (dash-dotted lines). The lower panel in the right plot show the ratio of observed data to estimated background. The shaded grey area shows the statistical uncertainty of the background estimate. [19]
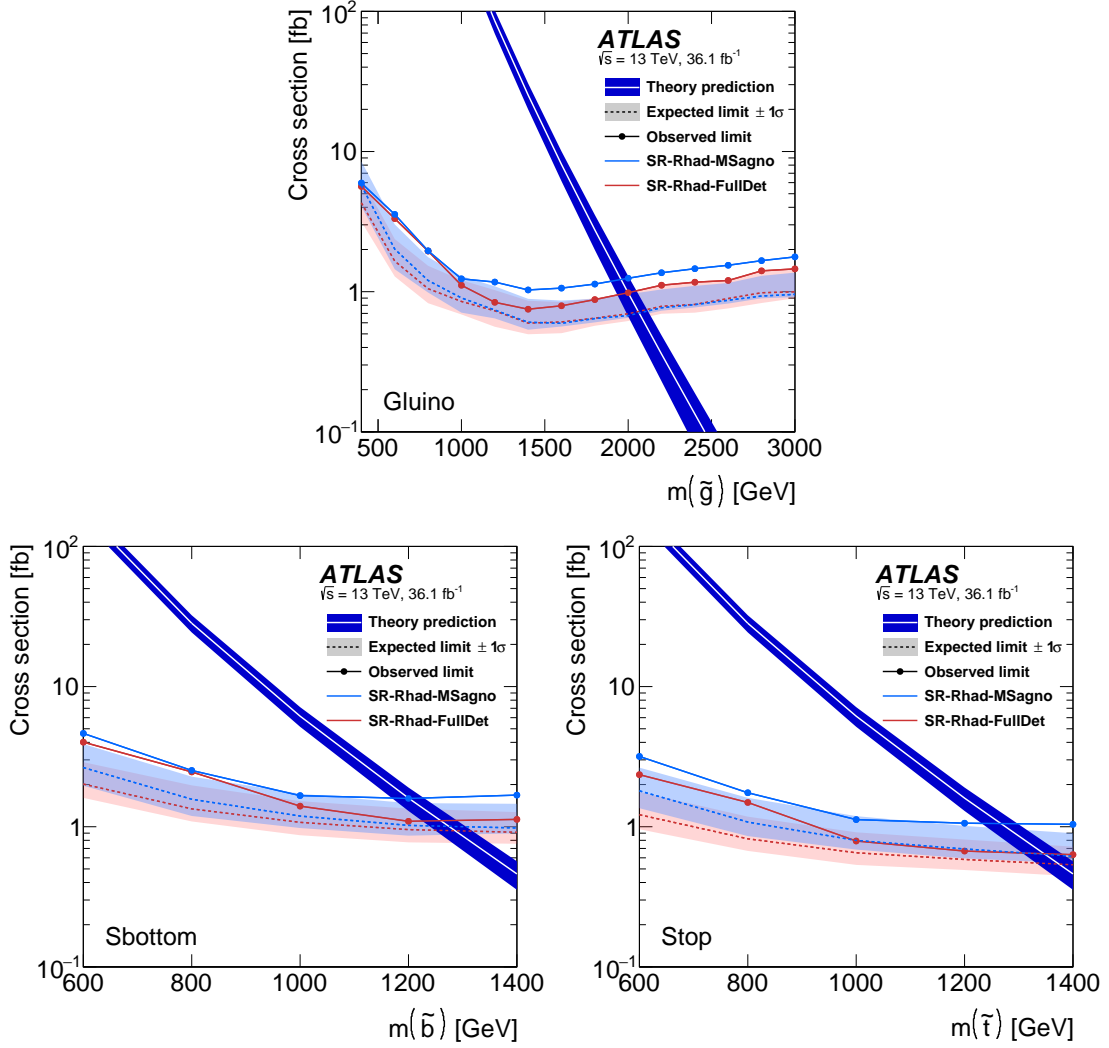
Figure 11: Expected (dashed lines) and observed (marked solid lines) upper cross-section limits in the gluino (top), sbottom (bottom-left) and stop (bottom-right) *R*-hadron searches, respectively, using two independent and not to be combined approaches being MS-agnostic (light blue) and using the full detector (red). The shaded light-blue/light-red bands represent the $\pm 1\sigma$ uncertainties in the expected limits. The theory prediction and its $\pm 1\sigma$ uncertainty are shown as a white line and a dark-blue band, respectively. [19]
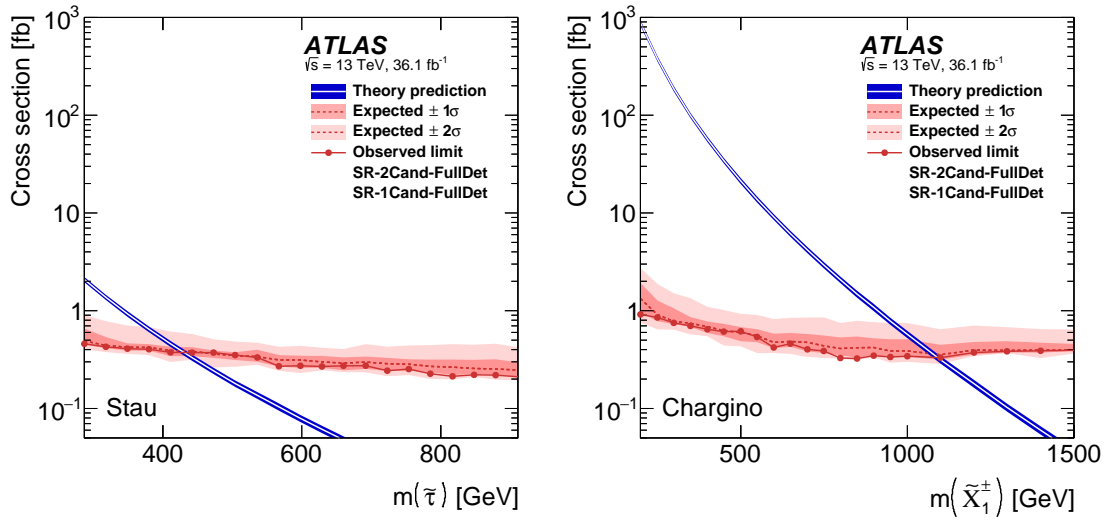
Figure 12: Expected (dashed red line) and observed (marked solid red line) upper cross-section limits using combined two- and one-candidate signal regions for stau pair production (left) and chargino pair production (right). The shaded dark-red (light-red) bands represent the $\pm 1\sigma$ ($\pm 2\sigma$) uncertainties in the expected limits. The theory prediction and its $\pm 1\sigma$ uncertainty are shown as a white line and a blue band, respectively.

5. Conclusion

Obviously this is just a glimpse of the results the ATLAS Collaboration has published on the subject of searches for LLPs. Some other recent results include a search for long-lived, massive particles in events with a displaced vertex and a displaced muon [31], a search for magnetic monopoles and stable high-electric-charge objects [32] and a search for heavy long-lived multicharged particles [33]. A complete overview on public results on all LLP searches as well as the full ATLAS physics programme can be found in Reference [34].

Until now, none of the highlighted or mentioned searches performed by the ATLAS Collaboration – or similar searches done by the CMS Collaboration, for that matter – have shown any significant deviation from background predictions in any of the signal regions, yet they place stringent limits on cross sections, particle masses and couplings of possible new physics scenarios. The ATLAS Collaboration is aiming to cover the vast signature and lifetime space of LLPs and further take advantage of the complementarity of prompt and displaced searches, with many updated and new results from Run-2 data still to come and a full Run 3 and the high-luminosity LHC still ahead.

References

[1] ATLAS Collaboration; *J. Instrum.* 3 (2008) S08003; 10.1088/1748-0221/3/08/S08003

[2] ATLAS Collaboration; submitted to *J. High Energy Phys*; arXiv:1905.09787

[3] M. Fukugita, T. Yanagidal; *Phys. Lett. B* 174 (1986) 45; 10.1016/0370-2693(86)91126-3

[4] T. Asaka, S. Blanchet, M. Shaposhnikov; *Phys. Lett. B* 631 (2005) 151;
10.1016/j.physletb.2005.09.070

[5] T. Asaka, M. Shaposhnikov; *Phys. Lett. B* 620 (2005) 17; 10.1016/j.physletb.2005.06.020

[6] L. Canetti, M. Drewes, M. Shaposhnikov; *Phys. Rev. Lett.* 110 (2013) 061801;
10.1103/PhysRevLett.110.061801

[7] ATLAS Collaboration; *ATL-PHYS-PUB-2019-013*; https://cds.cern.ch/record/2669425

[8] ATLAS Collaboration; *ATL-PHYS-PUB-2017-014*; https://cds.cern.ch/record/2275635

[9] DELPHI Collaboration; *Z. Phys. C* 74 (1997) 57; 10.1007/s002880050370

[10] ATLAS Collaboration; submitted to *Eur. Phys. J. C*; arXiv:1902.03094

[11] S. Chang, P.J. Fox, N. Weiner; *JHEP* 08 (2006) 068; 10.1088/1126-6708/2006/08/068

[12] M. J. Strassler, K.M. Zurek; *Phys. Lett. B* 651 (2007) 374; 10.1016/j.physletb.2007.06.055

[13] S. Chang, R. Dermisek, J.F. Gunion, N. Weiner; *Ann. Rev. Nucl. Part. Sci.* 58 (2008) 75;
10.1146/annurev.nucl.58.110707.171200

[14] M.J. Strassler, K.M. Zurek; *Phys. Lett. B* 661 (2008) 263; 10.1016/j.physletb.2008.02.008

[15] Y.F. Chan, M. Low, D.E. Morrissey, A. P. Spray; *JHEP* 05 (2012) 155; 10.1007/JHEP05(2012)155

[16] ATLAS Collaboration; *JINST* 11 (2016) P05013; 10.1088/1748-0221/11/05/P05013

[17] ATLAS Collaboration; *Phys. Rev. D* 99 (2019) 052005; 10.1103/PhysRevD.99.052005

[18] ATLAS Collaboration; *JHEP* 10 (2018) 031; 10.1007/JHEP10(2018)031

[19] ATLAS Collaboration; *Phys. Rev. D* 99 (2019) 092007; 10.1103/PhysRevD.99.092007

[20] C.F. Kolda; *Nucl. Phys. Proc. Suppl.* 62 (1998) 266; 10.1016/S0920-5632(97)00667-1

[21] G.F. Giudice, A. Romanino; *Nucl. Phys. B* 699 (2004) 65; 10.1016/j.nuclphysb.2004.11.048

[22] N. Arkani-Hamed, S. Dimopoulos, G. F. Giudice, A. Romanino; *Nucl. Phys. B* 709 (2005) 3;
10.1016/j.nuclphysb.2004.12.026

[23] M. Carena, D. Choudhury, R.A. Diaz, H.E. Logan, C.E.M. Wagner; *Phys. Rev. D* 66 (2002) 115010;
10.1103/PhysRevD.66.115010

[24] C. Balazs, M. Carena, C.E.M. Wagner; *Phys. Rev. D* 70 (2004) 015007;
10.1103/PhysRevD.70.015007

[25] M. Dine, W. Fischler; *Phys. Lett. B* 110 (1982) 227; 10.1016/0370-2693(82)91241-2

[26] L. Alvarez-Gaume, M. Claudson, M.B. Wise; *Nucl. Phys. B* 207 (1982) 96;
10.1016/0550-3213(82)90138-9

[27] C.R. Nappi, B.A. Ovrut; *Phys. Lett. B* 113 (1982) 175; 10.1016/0370-2693(82)90418-X

[28] M. Dine, A.E. Nelson; *Phys. Rev. D* 48 (1993) 1277; 10.1103/PhysRevD.48.1277

[29] M. Dine, A.E. Nelson, Y. Shirman; *Phys. Rev. D* 51 (1995) 1362; 10.1103/PhysRevD.51.1362

[30] M. Dine, A.E. Nelson, Y. Nir, Y. Shirman; *Phys. Rev. D* 53 (1996) 2658; 10.1103/PhysRevD.53.2658

[31] ATLAS Collaboration; *ATLAS-CONF-2019-006*; http://cdsweb.cern.ch/record/2668377

[32] ATLAS Collaboration; submitted to *Phys. Rev. Lett.*; arXiv:1905.10130

[33] ATLAS Collaboration; *Phys. Rev. D* 99 (2019) 052003; 10.1103/PhysRevD.99.052003

[34] ATLAS Collaboration; https://twiki.cern.ch/twiki/bin/view/AtlasPublic